Kimura et al. *NPG Asia Materials* (2022) 14:27
https://doi.org/10.1038/s41427-022-00372-w

NPG Asia Materials

ARTICLE Open Access

Gelation and anomalous viscosity dynamics in aqueous dispersions of synthetic hectorite

Yuji Kimura[1], Shoichi Shimizu[1] and Kazutoshi Haraguchi[1,2]

Abstract

Exfoliated clay nanosheets (CNSs) of synthetic hectorite (s-hectorite) have been used for synthesizing advanced functional materials and gels that exhibit high transparency, high mechanical toughness, and many unprecedented characteristics like optical anisotropy, cell harvesting, instant strong adhesion, and self-healing. Therefore, it is important to determine the rheological properties of aqueous s-hectorite dispersions in terms of the CNS microstructures formed in the dispersion. Herein, viscosity changes in aqueous dispersions of s-hectorite were determined using a vibration viscometer to measure viscosity under agitated and static conditions. Upon varying the pH and salt concentration, aqueous dispersions of s-hectorite exhibited a maximum viscosity accompanied by gelation. Additionally, the aqueous dispersion with maximum viscosity exhibited large and complex time-dependent viscosity changes in the static state after cessation of stirring. The anomalous viscosity dynamics depended on the types of clay, acid (salt), temperature, repetitions, and agitation conditions used. The mechanisms for viscosity dynamics have been discussed in terms of variations in the CNS microstructures. It is inferred that anomalous viscosity dynamics are a general phenomenon in multicomponent dispersion systems containing CNSs.

Introduction

Clays possess an array of unique properties, such as excellent ion-exchange capabilities, selective adsorption, intercalation, reinforcement, and catalytic activities owing to their layered, fibrous, or hollow crystal structures, as well as the occurrence of permanent charges on their surfaces[1]. In particular, clay minerals belonging to the smectite group, such as montmorillonite, hectorite, and saponite, have exfoliation abilities and have been widely used in many industries, such as cosmetics, catalysis, paper, paint, and ceramics[2]. Moreover, such clays have found applications as nanocomponents in the development of advanced functional materials with distinctive characteristics, such as low gas permeability, incombustibility, controlled mesoporosity, and excellent thermomechanical properties[3–6].

Clay minerals belonging to the smectite group exhibit 2:1 crystal structures comprising an octahedral layer of alumina or magnesia sandwiched between tetrahedral silica layers (Fig. S1a). They bear negative charges on their layered surfaces due to partial isomorphic substitution (e.g., $Mg^{2+} \rightarrow Li^{+}$: hectorite) and contain equivalent cations (e.g., Na^{+}) between their layers. Consequently, smectite clays can swell in water and gradually delaminate into discrete, disc-like nanoparticles (i.e., clay nanosheets (CNSs)) (Fig. S1b)[1,7]. The resulting CNSs have thicknesses of ~1 nm and diameters in the range of 20–1000 nm, depending on whether the clays were obtained from synthetic or natural sources. In particular, synthetic hectorite (s-hectorite, e.g., Laponite®-XLG) can be completely exfoliated to yield individual CNSs in water owing to its small crystal layer size ($\varphi \approx 30$ nm)[8,9] and adequate surface charge (104 meq/100 g).

Super hydrogels[10,11] and novel soft nanocomposites[12] with improved mechanical properties (e.g., high strength and large elongation)[13,14] and distinguished characteristics (e.g., large and rapid swelling/deswelling, new

Correspondence: Kazutoshi Haraguchi (haraguchi.kazutoshi@nihon-u.ac.jp)
[1]Department of Applied Molecular Chemistry, College of Industrial Technology, Nihon University, 1-2-1 Izumi-cho, Narashino, Chiba 275-8575, Japan
[2]GN Corporation Co Ltd, 3-8 Wakamatsu, Kofu 400-0866, Japan

stimuli sensitivity, unique changes in optical anisotropy, stem cell harvesting, biocompatibility, contractive force generation, instant strong adhesion, and self-healing)[13,15–18] have been developed using s-hectorite. Since then, aqueous dispersions of s-hectorite have received considerable attention because all the excellent properties and characteristics were derived from the unique polymer–clay (i.e., CNS) network structures formed by in situ polymerization in the presence of CNSs in aqueous media[12,13]. Therefore, it is important to evaluate the rheological characteristics of aqueous s-hectorite dispersions in terms of the CNS microstructures formed in the dispersion.

An aqueous dispersion of smectite clay is a typical colloidal dispersion whose rheological properties depend significantly on the concentration and microstructure of the nanoparticles (CNSs). When smectite clays are dispersed in water, the resulting aqueous dispersions typically exhibit thixotropic behavior due to formation of the so-called "house-of-cards" structure in the static state[1,7] and subsequent breakage when stress is applied[19,20] (Fig. S1c, d). Furthermore, above a certain clay concentration, the dispersion becomes a gel due to the formation of a continuous CNS network[7]. To date, the detailed rheological characteristics of smectite clay aqueous dispersions have been studied for natural montmorillonite[21–24], s-hectorite[25–31], and their mixtures[32]. Emphasis has been placed on the effects of clay concentration[25,26,28,29], pH[21,33,34], added salts[22,23,26], measurement time[24,35,36], gelation[27,37], fractal dimension[31], and flow instabilities in different flow regimes[28,38].

Among smectite clays, s-hectorite forms a uniform and transparent aqueous dispersion or hydrogel, and this characteristic plays an important role in conferring new functions to advanced materials and gels, as described above. Therefore, the aqueous dispersion of s-hectorite is best suited for studying the relationships between rheological properties and CNS microstructure. Herein, we report an investigation of the viscosity of aqueous s-hectorite dispersions using a vibration viscometer, with specific focus on the effects of pH and salt and the viscosity dynamics in the static state. To the best of our knowledge, these characteristics of aqueous s-hectorite dispersions have never been observed before.

Materials and methods

Materials

An s-hectorite, viz. Laponite®-XLG ($[Mg_{5.34}Li_{0.66}Si_8O_{20}(OH)_4]Na_{0.66}$; Rockwood Ltd., UK) supplied by Wilbur-Ellis Co. (Tokyo, Japan) and natural montmorillonite (n-montmorillonite, $[Al_{5.34}Mg_{0.66}Si_8O_{20}(OH)_4]Na_{0.66}$: Kunipia-F) supplied by Kunipia Industries Co. (Tokyo, Japan), were used as clays in this investigation. Laponite®-XLG was used after purification by washing with ethanol/water (90:10 w/w) and subsequent vacuum drying. Kunipia-F was further refined using the following procedure: the washed Kunipia-F was dispersed in water (5 wt%) with stirring for 24 h and subsequently allowed to stand for 24 h. Then, the supernatant dispersion was collected and vacuum-dried at 100 °C. The yield of refined Kunipia-F was approximately 65 wt% of that of pristine Kunipia-F. X-ray diffraction (XRD) profiles of purified s-hectorite (Laponite®-XLG) and n-montmorillonite (Kunipia-F) are shown in Fig. S2a, b, respectively. Ultrapure water supplied by a Puric-Mx system (Organo Co., Japan) was used in all experiments. Inorganic acids (6 N HCl, 6 N H_2SO_4), organic acids ($C_nH_{2n+1}COOH$: n = 0–7), alkali (6 N NaOH), salts (3 N NaCl, 3 N $CaCl_2$), poly (acrylic acid) (PAAc: M_w = 1,000,000), sodium poly (acrylic acid) (PAAcNa: M_w = 800,000), and polyethylene glycol (PEG: M_w = 1,000,000) were used without further purification. All the chemicals and polymers, except for PAAcNa (Polysciences, Inc., USA), were purchased from FUJIFILM Wako Pure Chemical Corp., Japan.

Preparation of aqueous smectite clay dispersions

Aqueous smectite clay (e.g., s-hectorite) dispersions with clay concentrations (C_{clay}) of 1.0–3.5 wt% were prepared by carefully mixing the clay with water and then stirring for 24 h at ambient temperature (20–25 °C). Ternary dispersions at different pH levels or salt concentrations (C_{salt}) and comprising smectite clay, water, and acid/alkali/salt were prepared by dropwise addition of various acid, alkali, or salt solutions to the original aqueous clay dispersions under stirring. For the aqueous smectite clay–polymer dispersion, aqueous solutions (10 wt%) of PAAc, PAAcNa, and PEG were added dropwise under stirring.

Measurements

Sample viscosities were measured at 25 °C using a sine-wave tuning-fork-type vibration viscometer (SV-10, A&D Co., Japan) calibrated with three standard solvents (kinematic viscosities: 10, 100, and 500 mm^2/s) and water. Viscosity was obtained by dividing the measured value by the density according to JIS Z 8803 (2011). Unless otherwise noted, the viscosity was typically measured for 5 min after the cessation of stirring (i.e., in the static condition), and the temperature was recorded simultaneously. Changes in viscosity under alternating stirring (5 min) and standing (15 min) conditions were recorded approximately 10 times. The aqueous clay dispersion was agitated, i.e., stirred by rotating a polytetrafluoroethylene (PTFE) rotor (8 mm φ × 40 mm length) in a glass sample container (60 mm φ × 65 mm height: sample liquid (180 ml)) at a predetermined rotation speed (100–500 rpm) (Fig. S3). The sample density was measured at 25 °C using a density meter (DA-130N, Kyoto Electronics Manufacturing Co.,

Japan). Ultrasonic waves (20 kHz, 5 W) generated using an ultrasonic device (SN-10, Daikyo Denshi, Japan) were also employed as an alternative method of agitation. The light transmittance (LT) and turbidity of the aqueous clay dispersion were measured at 600 nm using a UV–vis spectrophotometer (V-730iRM: JASCO Co., Japan) equipped with a quartz cell (10 mm × 10 mm × 30 mm) and a turbidity meter (H198703, Hanna Instruments, USA), respectively. XRD patterns were obtained using an X-ray diffractometer (D2 PHASER: Bruker Co., USA) with Cu-Kα radiation (30 kV, 10 mA).

Results and discussion

Viscosity measurements using a vibration viscometer

Viscometers can be classified into different types based on their measurement principle: falling ball-type, capillary-type, rotational-type, and vibration-type. All these viscometers are considered standard viscosity measurement tools according to JIS Z 8803 (2011) and ASTM D2162 (2013). Among them, the vibration viscometer is used to determine viscosity by controlling the amplitude of sensor plates immersed in a sample liquid, i.e., by measuring the electric current required to drive the sensor plates at a specific amplitude and constant frequency (Fig. S3). Because the amplitude varies in response to the quantity of the frictional force produced by viscidity between the sensor plates and sample liquid, the physical quantity measured by vibration viscometers is the kinematic viscosity. The absolute viscosity can be obtained by dividing the displayed value by the sample density. Specific details can be found in the literature[39]. The vibration viscometer (SV-10) used in this study provides a wide dynamic range (0.3–10,000 mPa·s), enabling measurements of viscosity changes during thixotropic processes that involve sol–gel transitions. High resolution was achieved by vibrating at a frequency of 30 Hz, which was equivalent to the eigen-frequency (resonance) of the detection system.

The rheological properties of aqueous smectite clay dispersions with different compositions and pH levels have been studied using other types of devices, such as capillary viscometers[22], Couette-type rotating viscometers[21,30], and cone–plate- or plate–plate-type rotating rheometers[24,25,28,29,35]. In this study, we used a vibration viscometer, which is a unique tool for measuring viscosity with small vibrations (±200 μm), thereby dispensing with the need for a large flow. Previously, we reported that similar to the other types of viscometers (e.g., Brookfield rotating and Ubbelohde), the vibration viscometer can accurately measure the viscosity for standard solutions with low and high viscosities[40]. Furthermore, we used a vibration viscometer to determine the abnormal excess viscosity that appeared in clay–alcohol–aqueous dispersions[40] and discover new aqueous solutions with lower viscosities than water for the first time in 147 years[41].

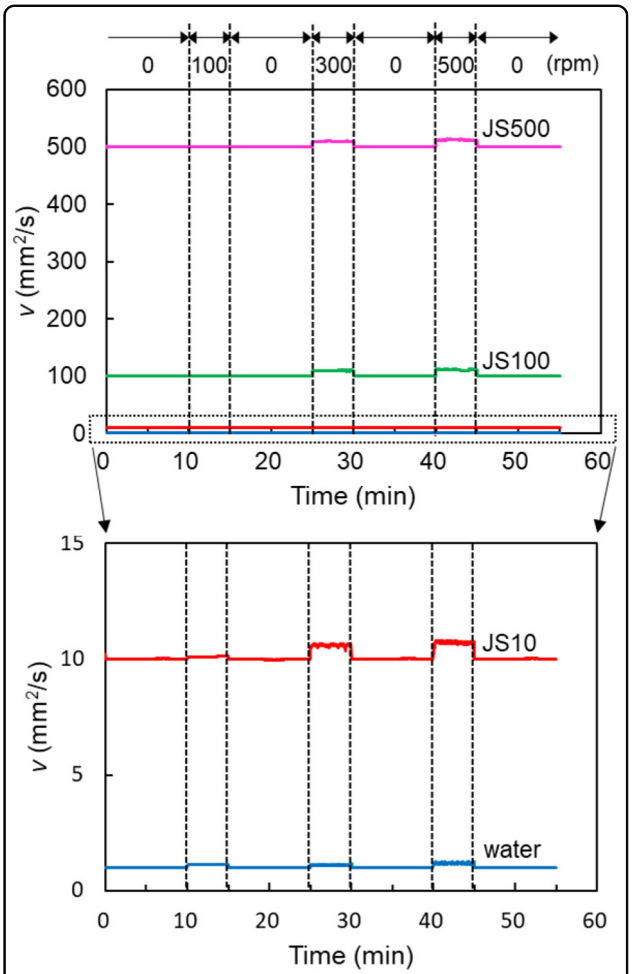

Fig. 1 Viscosity measurements using a tuning fork-type vibration viscometer. Kinematic viscosity (*ν*) was measured for standard solutions with different kinematic viscosities (10, 100, and 500 mm^2/s) and water (1.0 mm^2/s). Measurements were alternated between standing (0 rpm) and stirring at different rotational speeds (100, 300, and 500 rpm).

When the vibration viscometer was set up as shown in Fig. S3, the viscosity of the sample liquid could be measured under both static and stirring conditions, and the rotation speed of the PTFE rotor was electrically controlled. Therefore, time-dependent viscosity changes in the static state could be measured immediately after cessation of stirring, i.e., in the reconstruction processes of CNS microstructures. First, the effects of stirring and repetition on viscosity were measured using standard solutions without nanoparticles. As shown in Fig. 1, an accurate kinematic viscosity (*ν*) can be determined for all standard liquids (10–500 $mm^2\ s^{-1}$) and water (1.0 $mm^2\ s^{-1}$) in the static state regardless of the previous rotation speed (100–500 rpm). The measured value increased slightly during stirring, particularly at higher rotation speeds (probably due to water stream collisions with the

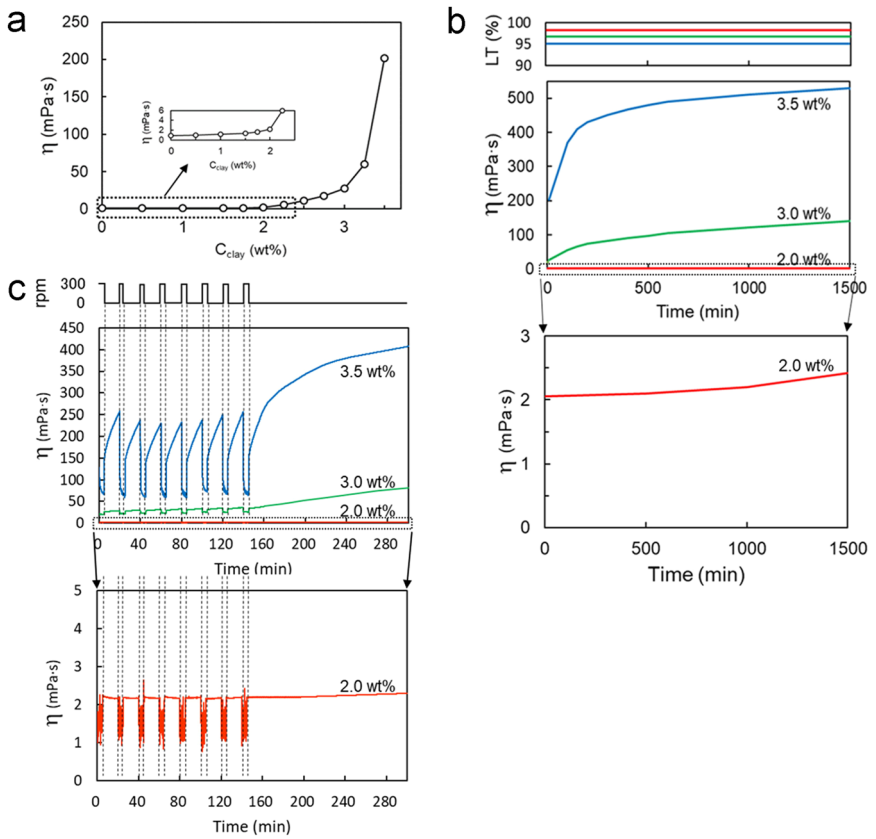

Fig. 2 Viscosities of aqueous s-hectorite dispersions with different clay concentrations. a Dependence of clay concentration (C_{clay}) on viscosity; **b** viscosity and light transmittance (LT) changes with standing time after cessation of stirring for aqueous s-hectorite dispersions with different C_{clay} values (2.0, 3.0, and 3.5 wt%); and **c** viscosity changes over repeated cycles of stirring (300 rpm, 5 min) and standing (0 rpm, 15 min) for aqueous s-hectorite dispersions with different C_{clay} values.

sensor plates); however, no practical change was observed after intermittent stirring was stopped. This step confirmed that the vibration viscometer can be used to track time-dependent changes in viscosity, if they occur, after the cessation of stirring; thus, the structural changes of CNSs in aqueous clay dispersions may be estimated.

Viscosity of aqueous s-hectorite dispersions

Owing to its moderate surface charge and small crystal layer size, s-hectorite (Laponite®-XLG) can be completely exfoliated in water[36,42] to obtain individual CNSs with diameters of 30 nm and heights of ~1 nm[8,26]. In the present study, the aqueous s-hectorite dispersion (C_{clay} = 2 wt%) was prepared under mild stirring for 24 h. The obtained dispersion was highly transparent and alkaline and had low viscosity (LT = 99%, turbidity = 10.1 NTU, pH 10.2, η = 2.2 mPa·s). As shown in Fig. 2a, the viscosity of the dispersion varied significantly depending on C_{clay} and increased steeply at concentrations exceeding 2 and 3 wt% because of the increased probability of CNS network formation in water. Furthermore, the viscosity of the aqueous dispersion gradually increased with time at rest (Fig. 2b) because of the formation and gradual buildup of a network of "house-of-cards" structures due to electrostatic attractions between faces (−) and edges (+)[1,7].

Figure 2c shows the changes in viscosity observed over repeated cycles of alternating stirring (300 rpm, 5 min) and rest (0 rpm, 15 min) for aqueous s-hectorite dispersions with different C_{clay} values. While relatively low viscosities were observed during stirring of dispersions with high C_{clay} values of 3 and 3.5 wt%, the viscosity values abruptly increased by approximately 10 and 100 mPa·s, respectively, upon cessation of stirring. Subsequently, the viscosity increased gradually over time and approached an asymptotic value, as shown in the last repeated measurement. This trend indicated that the CNS microstructure was destroyed during stirring and was partially reconstructed immediately upon cessation of stirring; subsequently, with increasing time at rest, the strength and/or network spread of the microstructure increased further. This long-term recovery for aqueous s-hectorite dispersion was consistent with those observed in previous studies using small amplitude oscillatory shear measurements[35]. Thus, an aqueous dispersion with C_{clay} = 3.5 wt%

showed a visibly clear sol–gel transition upon stirring and subsequent cessation. By contrast, for $C_{clay} = 2$ wt%, the viscosity increased only slightly (~0.5 mPa·s) upon cessation of stirring and increased very slowly during the subsequent rest condition, probably due to sluggish network formation (Fig. 2b, below). In contrast, the LT and turbidity of the aqueous dispersion did not change during stirring and subsequent standing even for a high C_{clay} dispersion (upper part of Fig. 2b). These results indicated that formation and breakage of the CNS microstructure and its associated network clearly caused a change in viscosity, but barely affected the LT and turbidity of the dispersion, which may be due to the very small size of the CNS unit and the high uniformity of the microstructure/network.

Variations in viscosity and transparency caused by altering the pH of aqueous smectite clay dispersions

The changes in viscosity, transparency, and pH of aqueous smectite clay dispersions were examined upon the addition of an acid or alkali. Figure 3a shows the changes in viscosity, LT, and turbidity of aqueous s-hectorite dispersion ($C_{clay} = 2$ wt%) as a function of pH. Here, the original (as-prepared) dispersion is shown with closed circles (pH 10.2). The pH was changed by adding 6 N HCl or 6 N NaOH, and the titration curve (relationship between pH and concentration of acid (C_{acid}: mM)) is shown in all related figures (Fig. 3a−d and Fig. 4). Notably, C_{clay} was not significantly changed (<0.05 wt%; upper part of Fig. 3a) due to the small quantities of added acid or alkali. In the alkaline pH range (pH 9–11), no changes in dispersion properties were observed, i.e., high LT (96%), low turbidity (10 NTU), and low viscosity (2 mPa·s) were retained. In contrast, the LT and turbidity rapidly decreased and increased, respectively, upon reducing the pH from 9 to 7. In addition, the viscosity exhibited a large change, with the maximum viscosity ($\eta_{max} = 1953$ mPa·s) observed at pH 7.9. In the acidic pH range (pH 6–7), the dispersion maintained a low viscosity, as well as low LT and high turbidity.

From the pH dependencies shown in Fig. 3a, it is evident that at pH 9 ($C_{HCl} = 2.5$ mM), CNSs began to form weak aggregates (agglomerates) that scattered light, and a concomitant steep increase in viscosity began. This point corresponded to the critical aggregation concentration (C_K)[43], which is indicated by a black arrow in all related images (i.e., Fig. 3a–d and Fig. 4). The number and/or size of CNS agglomerates increased upon addition of larger quantities of acid, and the viscosity exhibited a maximum behavior in the pH range 7–9. Specifically, η_{max}, which was significantly larger (~1000 times) than that of the original dispersion, appeared at pH 7.9. Furthermore, the dispersion showing η_{max} was translucent (LT 40% and turbidity 109 NTU) but uniform (i.e., no precipitation). These results indicated that network formation was dominant, i.e., CNS agglomerates formed the strongest network at pH 7.9. With a further decrease in pH to <7.9, the sizes and strengths of CNS aggregates were increased by strong interactions at lower pH, while the probability of network formation decreased. Finally, in the acidic state (pH < 7), aggregate sizes increased further while the viscosity remained low. These results are consistent with the rheological properties measured using a cone–plate rheometer[44], where the yield and shear modulus of the dispersions were decreased by altering the pH of the aqueous s-hectorite dispersion both in acidic and alkaline regions, and a maximum value was obtained at an intermediate pH of 8.2.

Next, the effect of acid type on the maximal viscosity behavior of the aqueous s-hectorite dispersion was examined. For this purpose, a variety of acids, including other inorganic acids (H_2SO_4), organic acids ($C_nH_{2n+1}COOH$: $n = 0$–7), and acidic polymers (PAAc), were employed. Evidently, each acid caused a steep increase in viscosity at C_K and a maximum viscosity at a specific pH. For H_2SO_4, changes similar to those obtained with HCl addition were observed over a slightly lower pH range (6.7–8.3), with C_K at pH 8.3 and η_{max} at pH 7.7 (Fig. 3b). For formic acid ($n = 0$), significant changes in the viscosity, turbidity, and LT were also observed (Fig. 3c), although both η_{max} (1056 mPa·s) and pH (7.1) at η_{max} were considerably lower than those obtained by using HCl. For the other organic acids examined ($n = 1$–7), the C_K (3.3–4.4 mM) and η_{max} (981–1095 mPa·s) were similarly observed at pH 7.6–8.3 and 7.0–7.3, respectively. The η_{max}, pH (η_{max}), $C_{\eta max}$ (acid concentration at η_{max}), and C_K values for all types of acids are summarized in Table 1. In general, all organic acids ($n = 0$–7) exhibited lower η_{max} values at lower pH and higher $C_{\eta max}$ and C_K than those for strong inorganic acids because of the relatively lower dissociation constant (i.e., higher pK_a (3.8–4.9)) of organic acids.

The acidic polymer (PAAc) (Fig. 3d) yielded a higher value of η_{max} (2341 mPa·s) and lower pH (7.1) at η_{max} than those in the HCl system. Thus, the viscosity behavior upon addition of acid (i.e., η began to increase at C_K and then exhibited a large maximum) was observed for many acids regardless of their chemical nature, e.g., organic and inorganic acids and acidic polymers. By contrast, for nonionic polymers like PAAcNa and PEG, the addition of the polymer to the aqueous s-hectorite dispersion resulted in entirely different changes in the viscosity, and no maximum viscosity was observed. Instead, a gradual increase in viscosity was observed upon increasing the amount of added polymer (Fig. 3e). Notably, the η_{max} in this system appeared after addition of a very small amount of PAAc (0.3 wt%), which was approximately 1/10 of the added amount of PAAcNa or PEG (~3 wt%) when η reached the same value.

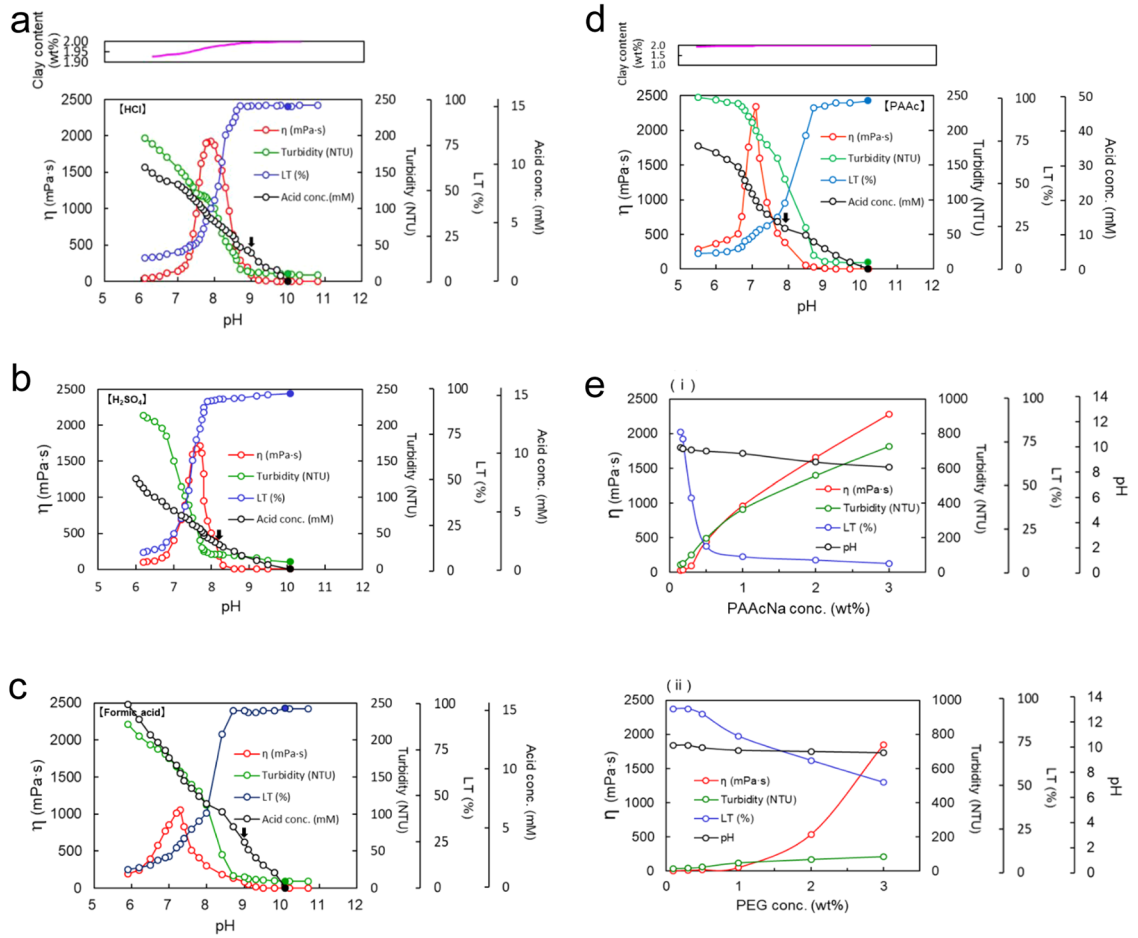

Fig. 3 Changes in the viscosity, light transmittance (LT), and turbidity for aqueous s-hectorite dispersions (C_{clay} = 2 wt%). Changes as a function of pH upon addition of **a** 6 N HCl, **b** 6 N H_2SO_4, **c** HCOOH, and **d** poly(acrylic acid) (PAAc) solution (10 wt%); **e** changes upon addition of a polymer; (i) sodium polyacrylate (PAAc–Na) solution (10 wt%), and (ii) poly(ethylene glycol) (PEG) solution (10 wt%). Titration curves (relationship between pH and concentration of acid (C_{acid}: mM)) are also shown in (**a**–**d**).

Next, the effect of the C_{clay} value (2.0, 2.5, and 3 wt%) was examined as a function of pH to determine its impact on the properties of the aqueous s-hectorite–HCl dispersion. A comparison of Figs. 3a, 4a, b revealed that a maximal viscosity appeared for the three dispersions. Meanwhile, all of the other factors (C_K, η_{max}, and pH (η_{max})) depended on the C_{clay} value: with an increase in C_{clay} from 2 to 3 wt%, C_K decreased from 2.5 mM to 1.0 mM, η_{max} increased from 1900 mPa·s to 6400 mPa·s, and pH at η_{max} increased from 7.9 to 8.9 (Table 1). All these changes in aqueous s-hectorite dispersions with different C_{clay} values can be attributed to the formation of an increasingly strong and widespread CNS network upon addition of a small amount of HCl with increasing C_{clay}.

The effects of different smectite clay types were also examined by using n-montmorillonite (Kunipia-F) (Fig. 4c). An aqueous n-montmorillonite–HCl dispersion (C_{clay} = 2 wt%) also exhibited a maximum viscosity; however, the values of η_{max} (417 mPa·s), pH (1.9) at η_{max}, pH (3.3) at C_K, and pH range (1–3.3) corresponding to the maximal viscosity were all much lower than those for the aqueous s-hectorite–HCl dispersions (dotted lines). The significantly low pH at C_K and the pH range for the maximal viscosity behavior in the aqueous Kunipia-F dispersion were attributed to the lower point at which the net charge on the Kunipia-F surface was zero compared with that on Laponite®XLG. Furthermore, the LT was 0% over the entire pH range. This is primarily attributed to insufficient exfoliation of n-montmorillonite in water and its large crystal sizes (~1000 nm).

The results described above indicated that the large change in viscosity observed upon altering the pH and the existence of a viscosity maximum at a specific pH are general phenomena observed for all aqueous smectite clay dispersions regardless of the type of acid and clay employed. However, among them, the aqueous s-

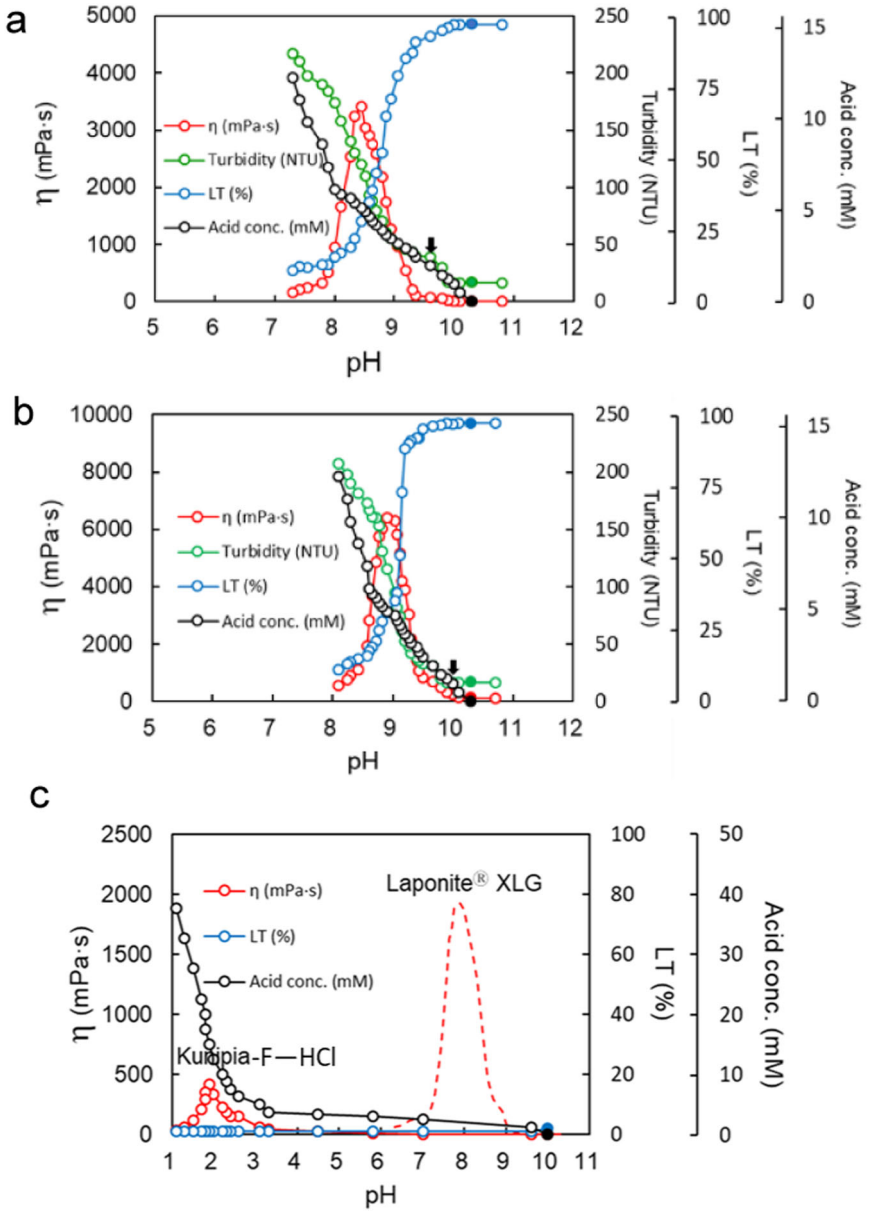

Fig. 4 Changes in viscosity, light transmittance (LT), and turbidity as a function of pH (HCl addition) for aqueous dispersions of smectite clay. a s-hectorite ($C_{clay} = 2.5$ wt%), **b** s-hectorite ($C_{clay} = 3$ wt%), **c** n-montmorillonite (Kunipia-F) ($C_{clay} = 2$ wt%). Titration curves (relationship between pH and concentration of acid (C_{acid}: mM)) are also shown in (**a**–**c**).

hectorite–acid dispersion exhibited the clearest changes in viscosity and LT due to full exfoliation into CNSs and the steady formation of a network in water.

Viscosity dynamics in aqueous s-hectorite dispersions

Time-dependent changes in the viscosities of aqueous smectite clay dispersions, especially aqueous s-hectorite–acid dispersions ($C_{clay} = 2$ wt%) that displayed η_{max} at a specific pH, were studied in the static state. In all the experiments, the viscosity measurements were repeatedly conducted with rotation speeds (time) alternating between 300 (5 min) and 0 rpm (15 min).

Aqueous s-hectorite–acid dispersions exhibited anomalous viscosity dynamics that were broadly classified into three types (0, I, and II) depending on the type of acid, as shown in Fig. 5. Types I and II exhibited large time-dependent viscosity changes after stirring was stopped. In type I, the maximum viscosity appeared immediately (within 1 min) after cessation of stirring. Subsequently, viscosity increased gradually and approached an

Table 1 pK_a values of various acids and η_{max}, pH at η_{max}, $C_{\eta max}$, C_K, and pH at C_K as evaluated from the pH dependence of η for s-hectorite–inorganic acid (HCl and H_2SO_4) or s-hectorite−organic acid ($C_nH_{2n+1}COOH$, $n = 0$–7) aqueous dispersions.

Acid	HCl ($C_{clay} = 2.0$ wt%)	HCl ($C_{clay} = 2.5$ wt%)	HCl ($C_{clay} = 3.0$ wt%)	H_2SO_4	*n* in $C_nH_{2n+1}COOH$							
					0	1	2	3	4	5	6	7
pKa	-3.00			−8.00	3.75	4.76	4.87	4.83	4.84	4.85	4.89	4.89
η_{max} (mPa·s)	1923	3419	6416	1714	1056	1025	981	1033	1095	976	1022	1032
pH [η_{max}]	7.90	8.46	8.90	7.70	7.05	7.20	7.10	7.03	6.99	7.25	7.20	7.26
C_{acid} [η_{max}] (mM)	5.53	5.27	5.02	3.61	7.30	6.99	6.91	6.54	6.24	6.41	6.22	6.20
C_K (mM)	2.51	2.01	1.00	2.01	3.31	4.40	4.01	3.27	4.14	3.60	4.15	3.78
pH [C_K]	9.00	9.60	10.00	8.30	8.80	8.00	7.60	7.80	8.30	7.90	8.20	7.80

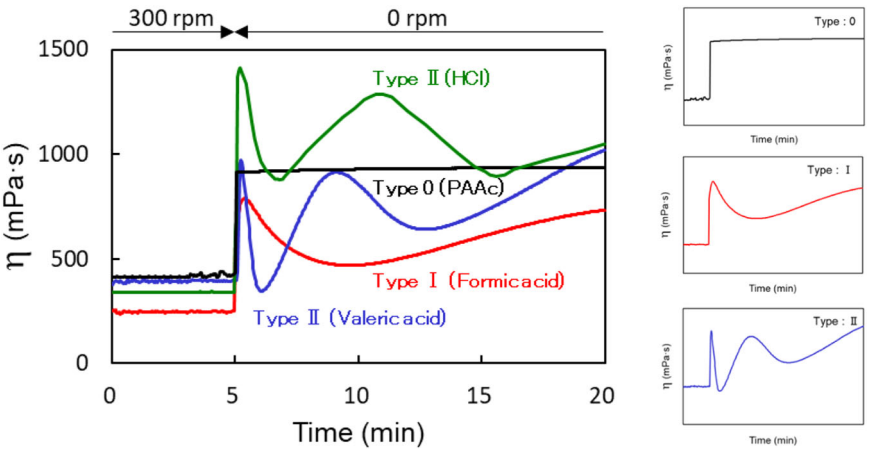

Fig. 5 Types of time-dependent viscosity changes. Types I and II exhibited one and two viscosity maxima, respectively, whereas Type 0 did not exhibit any viscosity maximum.

asymptotic value. In type II, two maximum viscosities were observed: the first viscosity peak appeared rapidly and lasted for 1 min, whereas the second peak was observed at 5–7 min. After the second peak, the viscosity increased again and approached an asymptotic value. By contrast, the corresponding time-dependent viscosity changes were not observed in type 0. The results for each type of acid and clay are described in the following subsections: organic acids, inorganic acids, and acidic and nonacidic polymers.

Organic acids

The time-dependent viscosity changes were measured for three aqueous s-hectorite–formic acid dispersions at pH 8.3, 7.3, and 6.3 (Fig. 6a). When the pH was 8.3 (transparent dispersion) or 6.3 (turbid dispersion), the dispersions were found to be typically thixotropic in all repeated measurements. By contrast, the translucent aqueous dispersion showing η_{max} (pH 7.3, $\eta_{max} =$ 1056 mPa·s, LT = 24%, and turbidity = 158 NTU: Fig. 3c) exhibited the time-dependent viscosity changes of type I (Fig. 5). The overall change in viscosity remained constant in all repeated measurements (Fig. 6a). On the other hand, the LT and turbidity of all aqueous s-hectorite–formic acid dispersions hardly changed throughout the repeated measurements.

Similar time-dependent viscosity changes were observed for the other organic acids ($C_nH_{2n+1}COOH$) ($n = 1$–7) in s-hectorite dispersion systems. Typical time-dependent viscosity changes resulting after nine iterations are shown in Fig. 6b for each organic acid ($n = 1$–7). At $n = 1$–3, the first viscosity peak appeared immediately after cessation of stirring (type I), whereas in the organic acids with longer alkyl chains ($n = 4$–7), the changes in viscosity changed to type II with the second η_{max}. This indicated that a complex viscosity change (type II) occurred when

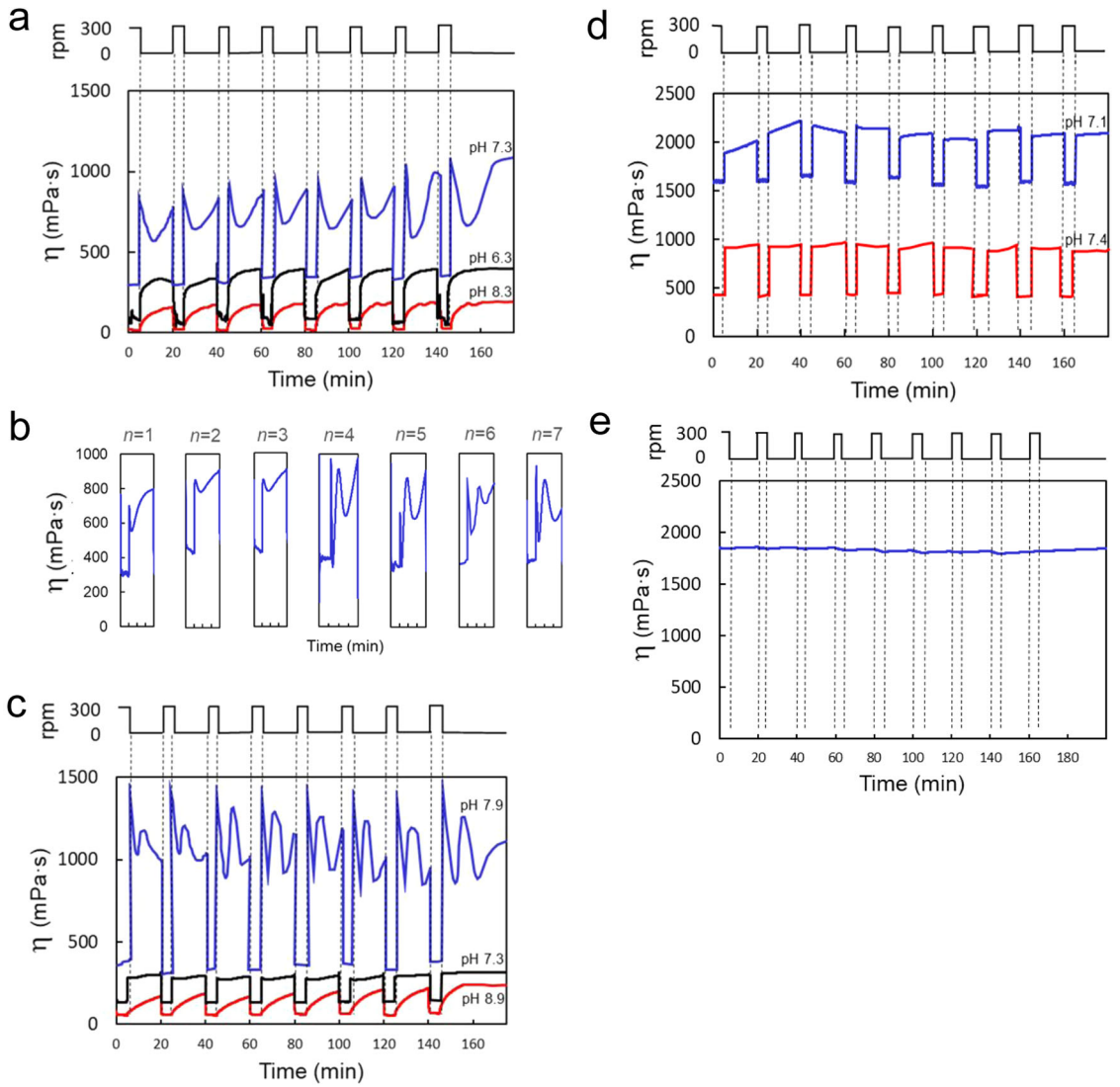

Fig. 6 Time-dependent viscosity changes for aqueous s-hectorite dispersions ($C_{clay} = 2$ wt%). Viscosity measurements were repeated with alternations between stirring (300 rpm, 5 min) and standing (0 rpm, 15 min) conditions. **a** s-Hectorite–formic acid aqueous dispersions with a pH of 7.3 (η_{max}); **b** ninth repeated measurements for s-hectorite–organic acid ($C_nH_{2n+1}COOH$, $n = 1$–7) aqueous dispersions; **c** s-hectorite–HCl aqueous dispersions with pH values of 8.9 and 7.9 ($pH_{\eta max}$), and 7.3. **d** s-hectorite–PAAc aqueous dispersions with pH 7.8 ($pH_{\eta max}$). **e** s-Hectorite aqueous dispersion comprising 3 wt% PEG.

organic acids with longer fatty chains were used, possibly resulting in the formation of complex nanostructures comprising CNSs and the acid at η_{max}.

Inorganic acids

Three aqueous s-hectorite–HCl dispersions ($C_{clay} =$ 2 wt%) at different pH levels of 8.9, 7.9 (η_{max}), and 7.3 were investigated under the same experimental conditions (Fig. 6c). The time-dependent viscosity changes depended strongly on pH, i.e., the aqueous dispersions at pH 8.9 and 7.3 exhibited simple thixotropic-type viscosity changes in all repeated runs. By contrast, the aqueous dispersion showing an η_{max} (pH 7.9) exhibited large, complex viscosity changes attributed to type II in the static state. Although the details of such viscosity changes are different for different numbers of repeated measurements, they converged to almost the same pattern with two viscosity maxima after the third repetition. In this study, the first viscosity peak appeared rapidly within 1 min, and the second maximum was observed at ~7 min. In terms of transparency, the LT was virtually unchanged throughout the repeated measurements. For aqueous s-hectorite–H_2SO_4 dispersions, similar viscosity changes were observed. These results indicated that a complex

microstructure showing a type II change was formed after several repetitions of stirring and standing in the s-hectorite–strong acid aqueous system.

Acidic and nonacidic polymers

The dispersion system comprising acidic polymer and s-hectorite showed viscosity change patterns that deviated completely from those observed for organic and inorganic acids. As shown in Figs. 5 and 6d, in all repeated experiments, aqueous PAAc–s-hectorite dispersions (C_{clay} = 2 wt%) with pH 7.1 (η_{max}) and pH 7.4 showed very large viscosities (1500 and 500 mPa·s, respectively) even during stirring, and the viscosities increased further to 2000 and 1000 mPa·s upon cessation of stirring. However, no complex time-dependent viscosity change (type 0) was observed after cessation of stirring regardless of the number of repeated runs. Thus, anomalous, large, and complex viscosity changes of types I and II were only observed when low-molecular-weight acids (organic and inorganic acids) were used. In comparison, the clay–PEG aqueous system did not show any viscosity change even during stirring (Fig. 6e) due to the uniformly mixed solution consisting of polymer (PEG), CNSs, and water.

Variations in viscosity and viscosity dynamics for aqueous s-hectorite–salt dispersions

The effects of added salt were investigated using a similar approach to that for added acids. Figure 7a, b show the changes in viscosity, LT, and turbidity for the aqueous s-hectorite dispersion (C_{clay} = 2 wt%) as a function of the concentrations of the two salts NaCl and $CaCl_2$. In both cases, although the pH changed slightly for every salt concentration range, large maximal viscosities and significant changes in LT and turbidity were observed within a specific range of C_{salt}. The C_K values above which the viscosity started to increase were 3.0 and 0.95 mM for NaCl and $CaCl_2$, respectively. Subsequently, the viscosities reached maximal values, i.e. 1408 mPa·s at 6.6 mM (NaCl) and 1425 mPa·s at 1.7 mM ($CaCl_2$), because the CNS agglomerates flocculated to form the strongest network at $C_{\eta max}$. Viscosity dynamics were also examined for the aqueous s-hectorite–salt dispersions showing η_{max} using a similar methodology to that for aqueous s-hectorite–acid dispersions. As shown in Fig. 7c (NaCl), a rather complex time-dependent viscosity change (type II) was observed before approaching an asymptotic value in equilibrium. This result also indicated the formation of a complex microstructure consisting of CNSs and NaCl at η_{max}.

Other factors responsible for viscosity dynamics

The anomalous viscosity dynamics observed for aqueous s-hectorite dispersions showing η_{max} must reflect changes in the CNS microstructures between the stirring/standing states. In this study, the effects of stirring conditions, stirring/standing interval, temperature, and the type of smectite clay were examined. Figure 8a shows the effect of rotation speed (100–500 rpm) on an aqueous s-

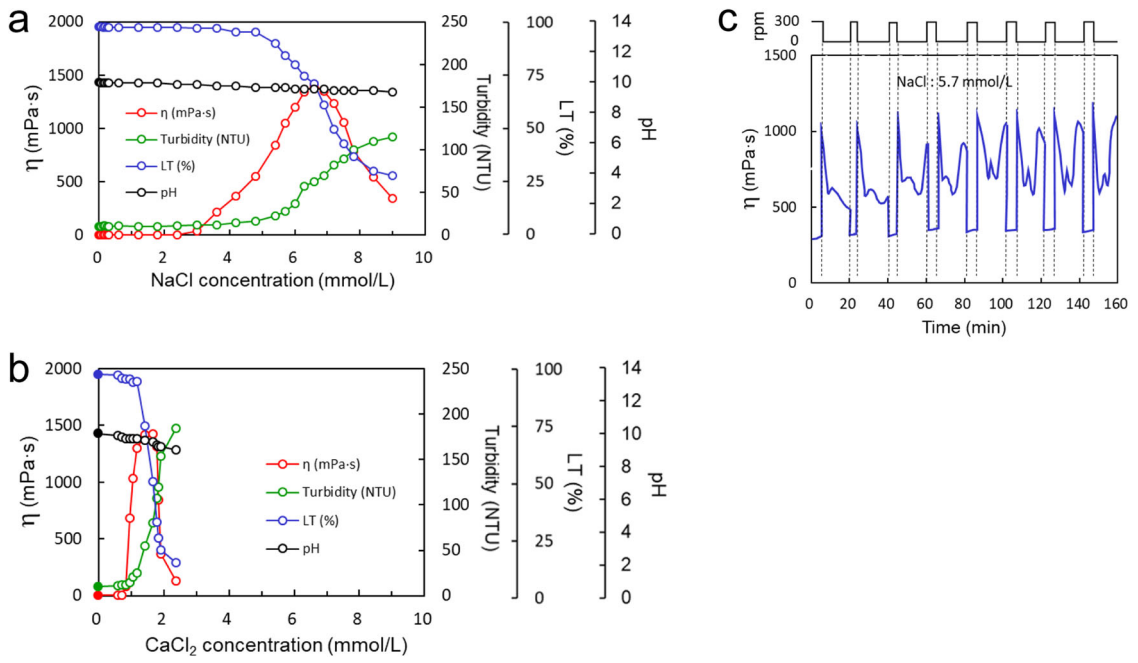

Fig. 7 Changes in viscosity, LT, turbidity, and pH as a function of salt concentration for aqueous s-hectorite dispersions (C_{clay} = 2 wt%). a NaCl, **b** $CaCl_2$. **c** Time-dependent viscosity changes for aqueous s-hectorite–salt dispersions with NaCl (5.7 mmol/L).

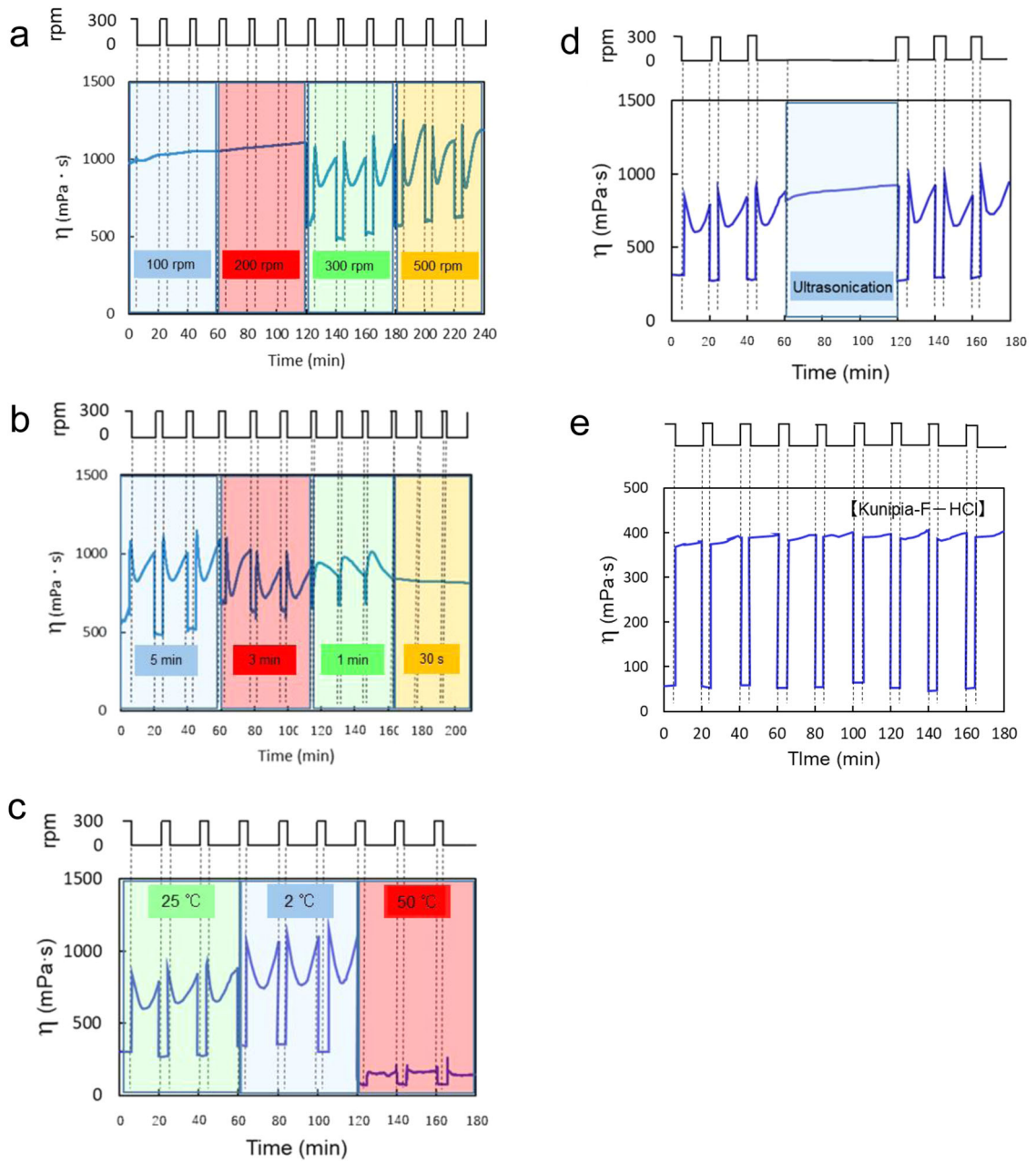

Fig. 8 Effects of various factors on time-dependent viscosity changes for aqueous smectite clay–formic acid dispersion showing η_{max}. a Rotation speed of the stirring rod (clay = s-hectorite); **b** length of the stirring time (clay = s-hectorite); **c** temperature (clay = s-hectorite); **d** type of agitation (ultrasonication) (clay = s-hectorite); and **e** type of smectite clay (clay = n-montmorillonite).

hectorite–formic acid dispersion at pH 7.3 (η_{max}). Typical time-dependent viscosity changes appeared when the rotational speed was 300 rpm at minimum. Conversely, if the speed was decreased to 200 rpm or less, both the reduction in viscosity during stirring and the viscosity change after cessation of stirring disappeared. This indicated that CNS microstructures and their networks were not destroyed in the upper part of the aqueous dispersion, near the sensor plate, upon mild stirring. Therefore, in this experimental setup (Fig. S3), a rotation speed threshold existed above which destruction of the network occurred.

Figure 8b shows the effect of stirring time in repeated measurements of the aqueous s-hectorite–formic acid dispersion (pH 7.3). Typical time-dependent viscosity changes were observed when the stirring time reached or exceeded 3 min, but no such changes were observed with stirring for 30 s in each repetition. With stirring for 1 min,

very simple viscosity changes were observed. These observations indicated that at the rotation speed used (300 rpm), the stirring time in the setup must exceed 3 min to sufficiently destroy CNS microstructures.

Regarding temperature effects, the time-dependent viscosity remained nearly unchanged when the experiments were performed at 50 °C or above (Fig. 8c), probably due to the thermal motion of the hydrated CNSs. In terms of the type of agitation, no time-dependent viscosity change was observed when the aqueous dispersion was subjected to ultrasonication (Fig. 8d). Finally, the effect of the smectite clay type on viscosity was examined using n-montmorillonite clay (Kunipia-F). During stirring, the aqueous n-montmorillonite–HCl dispersion ($C_{clay} = 2$ wt %) with a η_{max} (417 mPa·s) at pH 1.9 exhibited low viscosity, which rapidly recovered to high viscosity when stirring was ceased. No time-dependent viscosity change was observed during viscosity recovery (Fig. 8e). These phenomena are attributed to the destruction and rapid recovery of the network frame, i.e., the network was disconnected by stirring and reconnected instantaneously after cessation of stirring. However, its constituents (large aggregates of n-montmorillonite) were not decomposed by stirring.

Mechanisms of viscosity changes

All results obtained in this study must be correlated with changes in the dispersion/aggregation states of s-hectorite in aqueous media. Based on Derjaguin–Landau–Verwey–Overbeek (DLVO) theory[45], the original (as-prepared) aqueous dispersion of s-hectorite (charged colloidal particles) was stable due to the repulsive forces caused by overlapping diffusion electrical double layers (EDL) of individual CNSs in water. The viscosity of the original aqueous dispersion depended strongly on C_{clay} (Fig. 2a) because the CNSs formed a "house-of-cards" structure via electrostatic interactions between the surfaces (negative charge) and edges (polarized positive charge) of CNS (Fig. S1d) and formed a continuous network at high C_{clay}. Thus, the aqueous s-hectorite dispersion with C_{clay} values of 2–3 wt% exhibited simple thixotropic behavior (Fig. 2c) because the CNS network structure was broken under shear and reformed at rest.

The addition of acid or salt to aqueous sodium montmorillonite (2 wt%) dispersions characteristically influenced flow behavior, i.e., the flow values (shear stress and yield value) first decreased to a minimum and then increased steeply above C_K[43,46]. This minimum flow seen with low salt or acid concentrations was also observed in this study of the viscosity of aqueous s-hectorite (3 wt%) dispersions (Fig. 9a, b), and η decreased slightly from 125 mPa·s to 120 and 112 mPa·s at 0.12 mM NaCl and 0.19 mM HCl, respectively. These changes were minor compared with the changes in flow values reported in the literature because the flow was lower in the present study. On the other hand, the viscosity decrease was marginal when C_{clay} was 2 wt% (Fig. 9c, d) possibly because of the extremely low viscosity of the original dispersion (2 mPa·s). Similarly, the aqueous dispersion of Kunipia-F (3 wt%) showed a slight viscosity decrease (10 mPa·s → 8.5 mPa·s) at 8 mM NaCl (Fig. 9e). Mechanistically, the slight decrease in viscosity before C_K was presumably caused by a reduction in the secondary electroviscous effect[43]: increasing the acid (or salt) concentration would reduce the thicknesses of the diffuse ionic layers; thus, the viscosity would be diminished owing to reduced geometrical constraints.

Upon further addition of acid, the aqueous dispersion of s-hectorite exhibited large viscosity changes and showed a η_{max} at a specific pH (Fig. 3a–c and Fig. 4a, b). This is mainly because the variable charges at the edges of the CNSs changed from negative at high pH (through the ionization of Si–OH groups) to positive at low pH (through the addition of protons). Consequently, in alkaline solution, the repulsive EDL force between CNSs led to stable dispersion, and in acidic regions, CNSs were strongly aggregated by electrostatic attraction. At intermediate pH values, CNSs formed agglomerates, which flocculated to form networks. Model structures for two typical aggregations of CNSs at different pH levels, i.e., agglomerates at pH 7.9 (η_{max}) and aggregates at pH 7 in the s-hectorite (2 wt%)–HCl system, are depicted in Fig. 10a-1, b, respectively. In Fig. 10a-1, the agglomerates consisted of lightly accumulated CNSs, as suggested by the optical translucency; these agglomerates flocculated to form a widespread network (Fig. 10a-1N) in which the strength was significantly higher than that of the network in the original dispersion (Fig. S1d). By contrast, the aggregates in Fig. 10b (formed at pH 7) consisted largely of accumulated CNSs due to strong face-to-face cohesive interactions. Eventually, these aggregates exhibited low transparency and poor capability for network formation. Here, only CNSs are depicted in all models; for simplicity, the acidic ions (or salts) are not shown.

Based on the above models, the microstructural changes occurring in the stirring and subsequent standing states were estimated as follows (Fig. 10). When the aqueous dispersion was a gel consisting of a network of agglomerates (Fig. 10a-1, a-1N), the network decomposed to constituent agglomerates upon stirring (Fig. 10a-2 (with orientation): step 1); the viscosity was reduced because of disaggregation and orientation. When stirring was stopped, the disaggregated constituents suddenly gathered to form a tentative network (Fig. 10a-2*: step 2) via electrostatic attractions between the neighboring constituents and acidic ions, resulting in a rapid increase in viscosity. However, owing to the instabilities of these constituents at

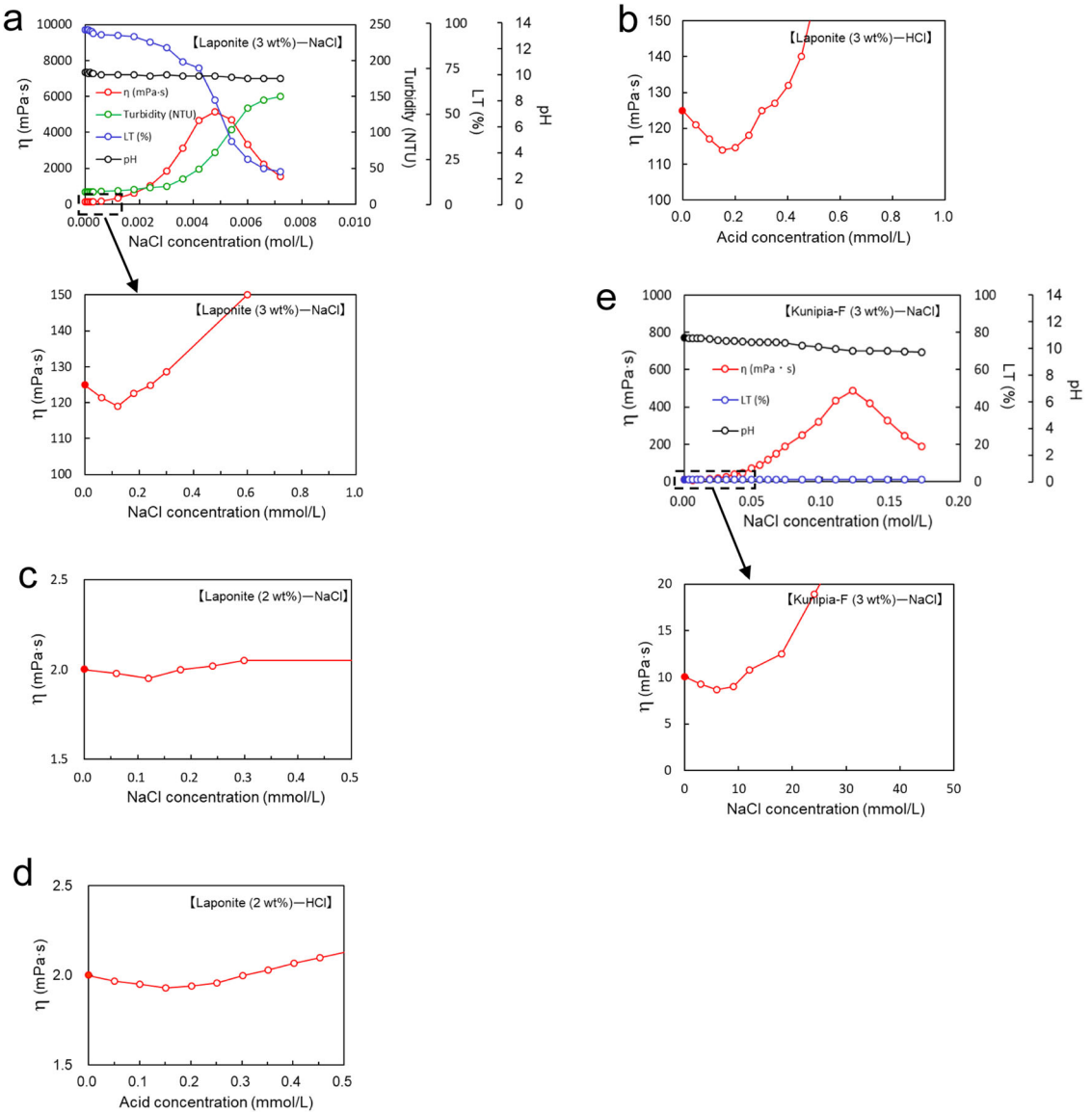

Fig. 9 Initial viscosity changes due to addition of salt or acid to aqueous clay dispersions. a s-hectorite (3 wt%)—NaCl; **b** s-hectorite (3 wt%)—HCl; **c** s-hectorite (2 wt%)—NaCl; **d** s-hectorite (2 wt%)—HCl; and **e** n-montmorillonite (3 wt%)—NaCl. Viscosity changes are shown only in detail in (**b**–**d**).

this pH, the components soon spontaneously separated from each other (Fig. 10a-2* → Fig. 10a-2 (no orientation): step 3), leading to a rapid decrease in viscosity and the first η_{max}. Subsequently, increasingly stable agglomerates were gradually formed and flocculated with each other to afford a stable network structure (Fig. 10a-1: step 4) with the passage of standing time; therefore, the viscosity gradually approached an asymptotic value at thermodynamic equilibrium. Pignon et al. studied the thixotropic behavior of aqueous s-hectorite dispersions using combinations of rheometric and scattering techniques[29]. They reported that under shear flow, the reduction in viscosity was due to disaggregation and orientation processes; during recovery, two different time scales corresponding to a rapid relaxation of the particle orientations and a slow aggregation process were identified. These previous findings were consistent with the results (steps 2–3 and 4) obtained in this study.

With vigorous stirring of the dispersion, the original network further decomposed into smaller components that included some individual CNSs (Fig. 10a-3 (with orientation): step 5). Therefore, spontaneous flocculation (i.e., tentative network formation) of decomposed units and subsequent destruction due to instability occurred

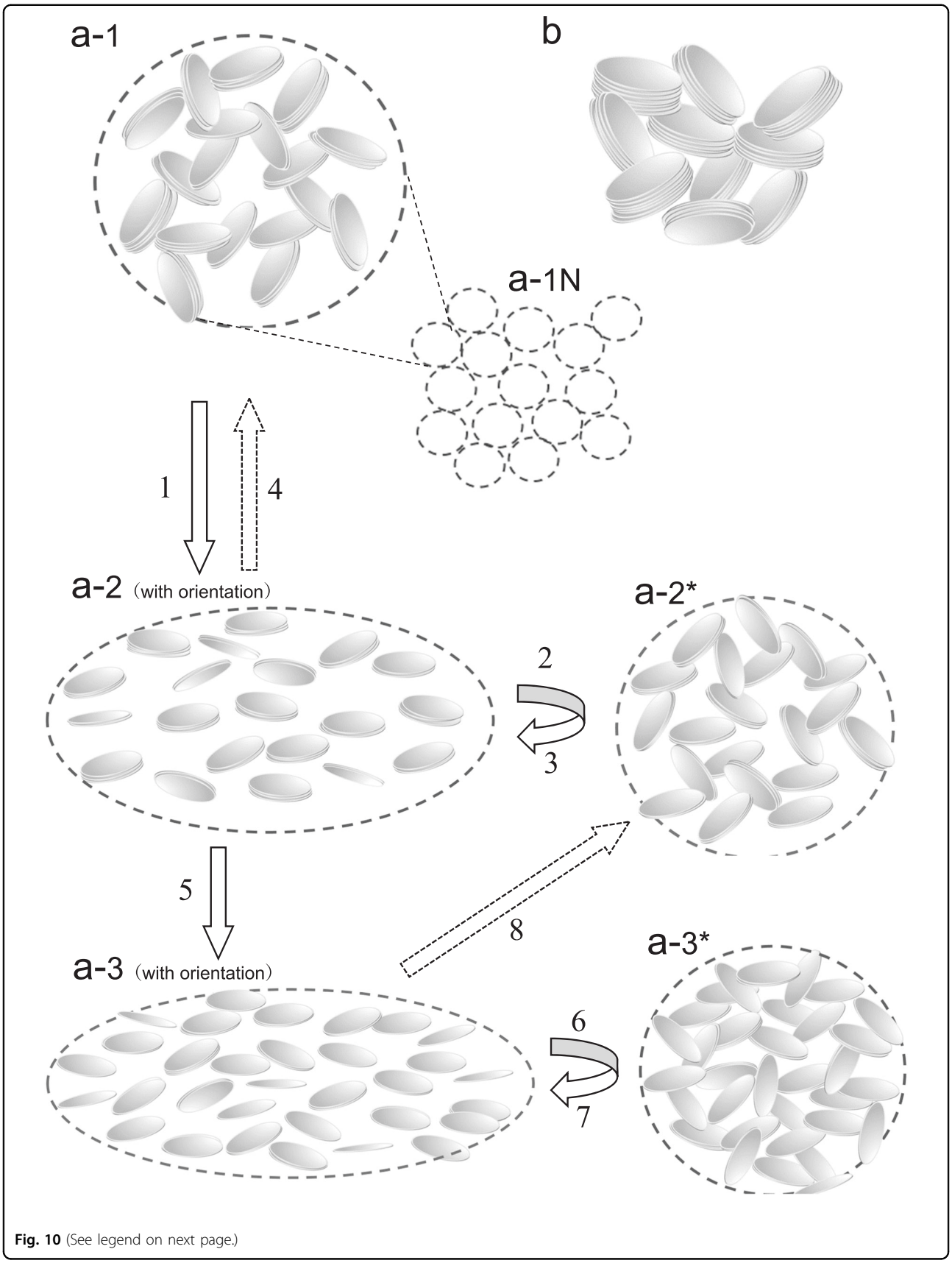

Fig. 10 (See legend on next page.)

(see figure on previous page)
Fig. 10 Schematic representations of model microstructures for aqueous s-hectorite dispersions. a-1 Agglomerates comprising weakly accumulated clay nanosheets (CNSs); **a-1N** network of agglomerates; **a-2** (with orientation) decomposed and oriented constituents of (**a-1**) formed upon stirring; **a-2*** tentative network consisting of decomposed constituents formed soon after cessation of stirring; **a-3** (with orientation) finely decomposed and oriented constituents of (**a-1**) formed upon vigorous stirring; **a-3*** Tentative network consisting of finely decomposed constituents formed soon after cessation of stirring; **b** large aggregates comprising strongly accumulated CNSs. In all models, only CNSs are depicted; for simplicity, acidic ions (or salts) are not shown.

twice (steps 6–7 and 8–3) in succession before the equilibrium network structure was achieved. Here, steps 2–3 and 6–7 occurred quickly (~1 min) because the phenomenon was associated with orientation, whereas steps 8–3 and 4 occurred more slowly (~10 and ~30 min, respectively) because they included reaggregation of the CNSs.

Under repeated stirring/standing, the degree of decomposition increased with increasing number of repetitions because the network was not completely reformed during 15 min of standing before the start of the next stirring treatment. Therefore, the viscosity changes converged to more complex changes with two viscosity peaks after several repeated runs (Fig. 6c). Furthermore, the pattern for time-dependent viscosity changes depended on the type of acid (Fig. 6a–d), which influenced the ease with which stirring caused network destruction. In particular, no practical time-dependent viscosity change was observed for PAAc (Fig. 6d) because the cationic polymer chain has many charged groups that interacted with numerous CNSs simultaneously; thus, complete separation by stirring was difficult to achieve. Thus, one or two viscosity peaks observed in the static state after the cessation of stirring were attributed to the tentative formation of a metastable network consisting of finely decomposed units. By contrast, little anomalous time-dependent viscosity change was observed when the clay was not fully exfoliated (e.g., n-montmorillonite: Fig. 8e) and when an acidic polymer was used (Fig. 6d). Furthermore, the aqueous s-hectorite–PEG (3 wt%) dispersion did not show any change throughout the stirring or standing processes (Fig. 6e). Thus, the large and complex time-dependent viscosity changes observed in the static state after cessation of stirring were only observed in multicomponent aqueous systems containing water, fully exfoliated CNSs, and low-molecular-weight inorganic or organic acids. The viscosity dynamics observed in this study will be further analyzed in terms of CNS microstructures by using small-angle scattering techniques (e.g., small-angle neutron scattering) or theoretical simulation techniques in future studies.

The addition of salt to an aqueous s-hectorite dispersion also influenced the changes in dispersion/aggregation states of CNSs, and consequently, the rheological properties (Fig. 7a, b). Based on DLVO theory[45], the addition of a salt leads to screening of the electrostatic repulsions between the charged particles (CNSs). Therefore, the s-hectorite–water system showed stable dispersion at zero or extremely low salt concentrations, which was also the case, i.e., $C_{NaCl} \leq 3$ mM and $C_{CaCl2} \leq 0.8$ mM in the present study. At higher C_{salt} values (beyond C_K), van der Waals attractions between CNSs dominated the electrostatic repulsion, and the resulting CNS agglomerates flocculated to form a strong network. Thus, the aqueous s-hectorite–salt dispersion was converted into a gel within a specific range of C_{salt}. Additionally, the aqueous s-hectorite–salt dispersions that showed η_{max} exhibited typical viscosity dynamics (type II), indicating that the network was composed of complex agglomerates consisting of CNSs and salt. Upon further addition of salt, the ionic strength of the dispersion considerably increased; subsequently, the viscosity decreased sharply owing to sedimentation of CNS aggregates; finally, no further viscosity dynamics were observed.

On the other hand, in aqueous s-hectorite–HCl dispersion systems with different C_{clay} values, both pH(C_K) and pH(η_{max}) increased with increasing C_{clay} (Table 1). For example, the aqueous dispersion with a C_{clay} value of 3 wt% exhibited the onset of viscosity increase and η_{max} at higher pH levels of 10 and 8.9, respectively, compared with those for the 2 wt% dispersion. This result may be due to the effects of the salt produced by neutralization with HCl. Thus, despite the system being in the alkaline range, the agglomeration of CNSs and network formation proceeded with an increase in C_{HCl}.

Interestingly, similar time-dependent viscosity changes were observed after cessation of stirring in our previous study on clay–ethanol–water dispersion systems (Fig. S4 (a part of Fig. 8c in the literature))[40]. The dispersion consisting of a specific composition of three components (ethanol, CNSs, and water) and showing a maximum viscosity exhibited time-dependent viscosity changes, although the mechanism for these changes was unknown. Based on the results obtained in this study, the time-dependent viscosity changes observed in our previous study may be attributed to spontaneous changes in the metastable microstructures upon cessation of stirring. Thus, the anomalous viscosity dynamics observed for the static state after stirring were confirmed to be a general phenomenon that occurs in multicomponent dispersion

systems containing nanoparticles with variable charges and anisotropic shapes (e.g., CNSs).

Conclusion

The viscosities of aqueous smectite clay dispersions were studied using a vibration viscometer, which can be used to measure the viscosity under both agitated and static conditions. This study was focused on aqueous s-hectorite dispersions consisting of fully exfoliated CNSs. The aqueous s-hectorite dispersion with low C_{clay} values (e.g., 2 wt%) formed a gel upon the addition of an acid or salt and showed a large η_{max}, which was ~1000 times that of the original dispersion, at a specific pH or salt concentration. The viscosities of the aqueous s-hectorite dispersion were reduced by stirring and recovered upon cessation of stirring. In particular, the aqueous dispersion showing η_{max} exhibited large and complex time-dependent viscosity changes after cessation of stirring. The viscosity dynamics strongly depended on the type of clay, acid, or salt used, as well as temperature, number of repetitions, and stirring conditions. Anomalous time-dependent viscosity changes exhibiting one or two viscosity maxima and a subsequent increase to an asymptotic value were observed in aqueous systems containing water, CNSs, and a low-molecular-weight acid or salt, as well as in other multicomponent dispersion systems including CNSs. The mechanism for the viscosity dynamics was discussed based on the microstructures of CNSs (re) formed in aqueous media. We believe that this study on aqueous clay dispersion and viscosity dynamics is important for understanding the unique behavior of clay nanosheets in aqueous media, as well as formulating rational designs of new functional materials. Furthermore, we infer that anomalous viscosity dynamics are general phenomena that may occur in multicomponent colloidal systems containing charged nanoparticles with anisotropic disc-like CNSs.

Acknowledgements
This work was financially supported by a Grant-in-Aid for Scientific Research (No. 18K05242) from the Japan Society of the Promotion of Science (JSPS).

Author contributions
K.H. planned the study, analyzed the results, and wrote the entire manuscript. Y.K. carried out all experiments under the supervision of K.H. and discussed the data with K.H. S.S. discussed the mechanism with K.H.

Conflict of interest
The authors declare no competing interests.

Publisher's note
Springer Nature remains neutral with regard to jurisdictional claims in published maps and institutional affiliations.

Supplementary information The online version contains supplementary material available at https://doi.org/10.1038/s41427-022-00372-w.

Received: 26 August 2021 Revised: 18 December 2021 Accepted: 11 February 2022.
Published online: 1 April 2022

References

1. Olphen, H. V. *An introduction to clay colloid chemistry* 2nd edn (John Wiley & Sons, New York, NY, USA, 1977).
2. Murray, H. H. Traditional and new applications for kaolin, smectite, and palygorskite: a general overview. *Appl. Clay Sci.* **17**, 207–221 (2000).
3. Lu, C. & Mai, Y.-W. Influence of aspect ratio on barrier properties of polymer-clay nanocomposites. *Phys. Rev. Lett.* **95**, 088303 (2005).
4. Ahmed, L., Zhang, B., Hatanaka, L. C. & Mannan, M. S. Application of polymer nanocomposites in the flame retardancy study. *J. Loss Prev. Process Ind.* **55**, 381–391 (2018).
5. Inagaki, S., Fukushima, Y. & Kuroda, K. Synthesis of highly ordered mesoporous materials from a layered polysilicate. *J. Chem. Soc. Chem. Comm.* **8**, 680–682 (1993).
6. Okada, A. & Usuki, A. Twenty years of polymer-clay nanocomposites. *Macromol. Mater. Eng.* **291**, 1449–1476 (2006).
7. Dijkstra, M., Hansen, J.-P. & Madden, P. A. Statistical model for the structure and gelation of smectite clay suspensions. *Phys. Rev. E* **55**, 3044 (1997).
8. Avery, R. G. & Ramsey, J. D. F. Colloidal properties of synthetic hectorite clay dispersions: II. Light and small angle neutron scattering. *J. Colloid Interface Sci.* **109**, 448–454 (1986).
9. Thompson, D. W. & Butterworth, J. T. The nature of laponite and its aqueous dispersions. *J. Colloid Interface Sci.* **151**, 236–243 (1990).
10. Haraguchi, K. & Takehisa, T. Nanocomposite hydrogels: a unique organic–inorganic network structure with extraordinary mechanical, optical, and swelling/de-swelling properties. *Adv. Mater.* **14**, 1120–1124 (2002).
11. Wang, Q. et al. High-water-content mouldable hydrogels by mixing clay and a dendritic molecular binder. *Nature* **463**, 339–343 (2010).
12. Haraguchi, K., Ebato, M. & Takehisa, T. Polymer–clay nanocomposites exhibiting abnormal necking phenomena accompanied by extremely large reversible elongations and excellent transparency. *Adv. Mater.* **18**, 2250–2254 (2006).
13. Haraguchi, K. Synthesis and properties of soft nanocomposite materials with novel organic/inorganic network structures. *Polym. J.* **43**, 223–241 (2011).
14. Li, H.-J., Jiang, H. & Haraguchi, K. Ultrastiff, thermoresponsive nanocomposite hydrogels composed of ternary polymer–clay–silica networks. *Macromolecules* **51**, 529–539 (2018).
15. Haraguchi, K. Soft nanohybrid materials consisting of polymer–clay networks. *Adv. Polym. Sci.* **267**, 187–248 (2015).
16. Haraguchi, K., Kimura, Y. & Shimizu, S. Reversible generation of large retractive tensile forces in isometric chemo-mechanical actuators composed of nanocomposite hydrogels and aqueous NaCl solutions. *Soft Matter* **14**, 927–933 (2018).
17. Haraguchi, K., Shimizu, S. & Tanaka, T. Instant strong adhesive behavior of nanocomposite gels toward hydrophilic porous materials. *Langmuir* **34**, 8480–8488 (2018).
18. Haraguchi, K., Uyama, K. & Tanimoto, H. Self-healing in Nanocomposite Hydrogels. *Macromol. Rapid Commun.* **32**, 1253–1258 (2011).
19. Cheng, D. C.-H. Thixotropy. *Int. J. Cosmet. Sci.* **9**, 151–191 (1987).
20. Mewis, J. Thixotropy—a general review. *J. Non-Newton. Fluid Mech.* **6**, 1–20 (1979).
21. Brandenburg, U. & Lagaly, G. Rheological properties of sodium montmorillonite dispersions. *Appl. Clay Sci.* **3**, 263–279 (1988).
22. Miyahara, K., Adachi, Y. & Nakaishi, K. The viscosity of a dilute suspension of sodium montmorillonite in an alkaline state. *Colloids Surf., A* **131**, 69–75 (1998).
23. Abend, S. & Lagaly, G. Sol–gel transitions of sodium montmorillonite dispersions. *Appl. Clay Sci.* **16**, 201–227 (2000).
24. Bekkour, K., Leyama, M., Benchabane, A. & Scrivener, O. Time-dependent rheological behavior of bentonite suspensions: An experimental study. *J. Rheol.* **49**, 1329–1345 (2005).
25. Pujala, R. K. & Bohidar, H. B. Slow dynamics, hydration and heterogeneity in laponite dispersions. *Soft Matter* **9**, 2003–2010 (2013).
26. Mourchid, A., Delville, A., Lambard, J., LeColier, E. & Levitz, P. Phase diagram of colloidal dispersions of anisotropic charged particles: Equilibrium properties, structure, and rheology of laponite suspensions. *Langmuir* **11**, 1942–1950 (1995).

27. Mourchid, A. & Levitz, P. Long-term gelation of laponite aqueous dispersions. *Phys. Rev. E* **57**, R4887 (1998).
28. Pignon, F., Magnin, A. & Piau, J.-M. Thixotropic colloidal suspensions and flow curves with minimum: Identification of flow regimes and rheometric consequences. *J. Rheol.* **40**, 573–587 (1996).
29. Pignon, F., Magnin, A. & Piau, J.-M. Thixotropic behavior of clay dispersions: combinations of scattering and rheometric techniques. *J. Rheol.* **42**, 1349–1373 (1998).
30. Bienia, M., Danglade, C., Lecomte, A., Brevier, J. & Pagnoux, C. Cylindrical couette flow of laponite dispersions. *Appl. Clay Sci.* **162**, 83–89 (2018).
31. Pignon, F., Piau, J.-M. & Magnin, A. Structure and pertinent length scale of a discotic clay gel. *Phys. Rev. Lett.* **76**, 4857–4860 (1996).
32. Pujala, R. K., Pawar, N. & Bohidar, H. B. Universal sol state behavior and gelation kinetics in mixed clay dispersions. *Langmuir* **27**, 5193–5203 (2011).
33. Lott, M. P. & Williams, D. J. A. The elastic properties of sodium montmorillonite suspensions. *Colloid Polym. Sci.* **274**, 43–48 (1996).
34. Benna, M., Kbir-Ariguib, N., Magnin, A. & Bergaya, F. Effect of pH on rheological properties of purified sodium bentonite suspensions. *J. Colloid Interface Sci.* **218**, 442–455 (1999).
35. Willenbacher, N. Unusual thixotropic properties of aqueous dispersions of laponite RD. *J. Colloid Interface Sci.* **182**, 501–510 (1996).
36. Ruzicka, B. et al. Observation of empty liquids and equilibrium gels in a colloidal clay. *Nat. Mater.* **10**, 56–60 (2011).
37. Dijkstra, M., Hansen, J. P. & Madden, P. A. Gelation of a clay colloid suspension. *Phys. Rev. Lett.* **75**, 2236 (1995).
38. Schmitt, V., Marques, C. M. & Lequeux, F. Shear-induced phase separation of complete fluids: The role of flow-concentration coupling. *Phys. Rev. E* **52**, 4009 (1995).
39. Goodwin, A. R. H. et al. A vibrating edge supported plate, fabricated by the methods of micro electro mechanical system for the simultaneous measurement of density and viscosity: results for methylbenzene and octane at temperatures between (323 and 423) K and pressures in the range (0.1 to 68) MPa. *J. Chem. Eng. Data* **51**, 190–208 (2006).
40. Kimura, Y. & Haraguchi, K. Clay—alcohol—water dispersions: Anomalous viscosity changes due to network formation of clay nanosheets induced by alcohol clustering. *Langmuir* **33**, 4758–4768 (2017).
41. Haraguchi, K. & Kimura, Y. New aqueous solutions with lower viscosities than water. *Bull. Chem. Soc. Jpn.* **94**, 1185–1191 (2021).
42. Morvan, M., Espinat, D., Lambard, J. & Zemb, T. H. Ultrasmall- and small-angle X-ray scattering of smectite clay suspensions. *Colloids Surf. A: Physicochemical Eng. Asp.* **82**, 193–203 (1994).
43. Penner, D. & Lagaly, G. Influence of anions on the rheological properties of clay mineral dispersions. *Appl. Clay Sci.* **19**, 131–142 (2001).
44. Ishijima, H., Kudo, M. & Masuko, T. Effect of pH on rheological properties of synthetic hectorite/water suspensions. *Nihon Reorojī Gakkaishi* **28**, 79–83 (2000).
45. Hiemenz, P. C. & Rajagopalan, R. *Principles of Colloid and Surface Chemistry*, 3rd ed. (Marcel Dekker, New York, 1997).
46. Permien, T. & Lagaly, G. The rheological and colloidal properties of bentonite dispersions in the presence of organic compounds IV. Sodium montmorillonite and acids. *Appl. Clay Sci.* **9**, 251–263 (1994).